Technical Note

First Observations of Mars Atmosphere and Ionosphere with Tianwen-1 Radio-Occultation Technique on 5 August 2021

Xiong Hu [1,*] , Xiaocheng Wu [1], Shuli Song [2], Maoli Ma [2], Weili Zhou [2], Qingchen Xu [1], Lei Li [1], Cunying Xiao [3], Xie Li [4], Chi Wang [1], Qinghui Liu [2], Lue Chen [4], Guangming Chen [4], Jianfeng Cao [4] , Mei Wang [4], Peijia Li [2], Zhanghu Chu [2], Bo Xia [2], Junfeng Yang [1], Cui Tu [1], Dan Liu [1,5], Simin Zhang [1,5], Quan Zhang [1,5] and Zheng Li [1]

[1] National Space Science Center, State Key Lab of Solar Activity and Space Weather, The Chinese Academy of Sciences, Beijing 100190, China; xcwu@nssc.ac.cn (X.W.); xqc@nssc.ac.cn (Q.X.); lil@nssc.ac.cn (L.L.); cw@spaceweather.ac.cn (C.W.); yangjunfeng@nssc.ac.cn (J.Y.); tucui@nssc.ac.cn (C.T.); liudan@nssc.ac.cn (D.L.); zhangsimin19@mails.ucas.ac.cn (S.Z.); zhangquan20@mails.ucas.ac.cn (Q.Z.); lizheng182@mails.ucas.ac.cn (Z.L.)

[2] Shanghai Astronomy Observatory, The Chinese Academy of Sciences, Shanghai 200030, China; slsong@shao.ac.cn (S.S.); mamaoli@shao.ac.cn (M.M.); wlzhou@shao.ac.cn (W.Z.); liuqh@shao.ac.cn (Q.L.); pjli@shao.ac.cn (P.L.); chuzhanghu@shao.ac.cn (Z.C.); bxia@shao.ac.cn (B.X.)

[3] Department of Astronomy, Beijing Normal University, Beijing 100875, China; xiaocunying@bnu.edu.cn

[4] Beijing Aerospace Flight Control Center, Beijing 100094, China; lixie_afdl@163.com (X.L.); luechen0912@163.com (L.C.); chen_g_m@126.com (G.C.); jfcao@foxmail.com (J.C.); wm2004xijiao@163.com (M.W.)

[5] University of the Chinese Academy of Sciences, Beijing 100049, China

* Correspondence: xhu@nssc.ac.cn; Tel.: +86-010-62582893

Abstract: The radio-occultation technique can provide vertical profiles of planetary ionospheric and atmospheric parameters, which merit the planetary-climate and space-weather scientific research so far. The Tianwen-1 one-way single-frequency radio-occultation technique was developed to retrieve Mars ionospheric and atmospheric parameters. The first radio-occultation event observation experiment was conducted on 5 August 2021. The retrieved excess Doppler frequency, bending angle, refractivity, electron density, neutral mass density, pressure and temperature profiles are presented. The Mars ionosphere M1 (M2) layer peak height is at 140 km (105 km) with a peak density of about 3.7×10^{10} el/m^3 (5.3×10^{10} el/m^3) in the retrieved electron-density profile. A planetary boundary layer (-2.35 km~5 km), a troposphere (temperature decreases with height) and a stratosphere (24 km–40 km) clearly appear in the retrieved temperature profile below 50 km. Results show that Tianwen-1 radio occultation data are scientifically reliable and useful for further Mars climate and space-weather studies.

Keywords: Tianwen-1; radio occultation; Mars ionosphere; Mars atmosphere; electron density; temperature; pressure; refractivity; neutral density

1. Introduction

The radio-occultation (RO) technique is a powerful and esoteric technique for exploring planetary ionospheres and atmospheres and has been commonly used in previous planetary missions, including a comet mission [1–4], since Mariner 4 reached Mars in 1965 [5]. During RO event observations, the spacecraft transmits a radio signal such that it propagates through the planet's atmosphere and ionosphere and arrives at the receiver on the Earth ground station. The refraction of the radio signal due to the planet's atmosphere and ionosphere is measured and used to derive the vertical profiles of the refractivity, and hence the corresponding neutral mass density, temperature, pressure and the ionospheric plasma density can be obtained, which is useful for the scientific studies of planetary climate and space weather.

Tianwen-1 is the first Chinese spacecraft exploring Mars [6,7] and was launched in 12:41 on 23 July 2020. Tianwen-1 entered orbit around Mars on 10 February 2021 (http://spacenews.com/chinas-tianwen-1-enters-orbit-sround-mars, accessed on 17 Feburary 2022). Like the previous Mars mission, the X-band radio link between Tianwen-1 and the deep-space ground stations on Earth allows the radio-occultation (RO) technique to be applied in retrieving Mars atmosphere and ionosphere profile data.

The first radio-occultation event data were achieved with the radio link between Tianwen-1 and the Shanghai VLBI (very long baseline interferometry) ground station (31°N, 121°E; geographic) on 5 August 2021. The Mars neutral atmosphere and ionosphere profiles with the Tianwen-1 RO technique are firstly derived and analyzed in this paper. Section 2 gives the Tianwen-1 RO technique description. Section 3 shows results of the initial profiles and analysis for atmosphere and ionosphere, respectively. Section 4 draws a conclusion.

2. Tianwen-1 Radio-Occultation Technique and Data

Unlike most two-way dual-frequency RO techniques [8–10], the Tianwen-1 RO technique here is based on the one-way single-frequency technique as described in the literature [11]. The details of the Tianwen-1 RO technique are given below.

2.1. One-Way Single-Frequency Radio Link between Tianwen-1 and Shanghai VLBI Ground Station

Tianwen-1 can receive and transmit radio signals at the X-band. The ground station with an antenna of 25 m aperture in Shanghai can be used to receive the downlink X-band radio signals. The one-way single-frequency link at the X-band is thus established by transmitting the X-band downlink from Tianwen-1 spacecraft to the Shanghai ground station, as depicted in Figure 1.
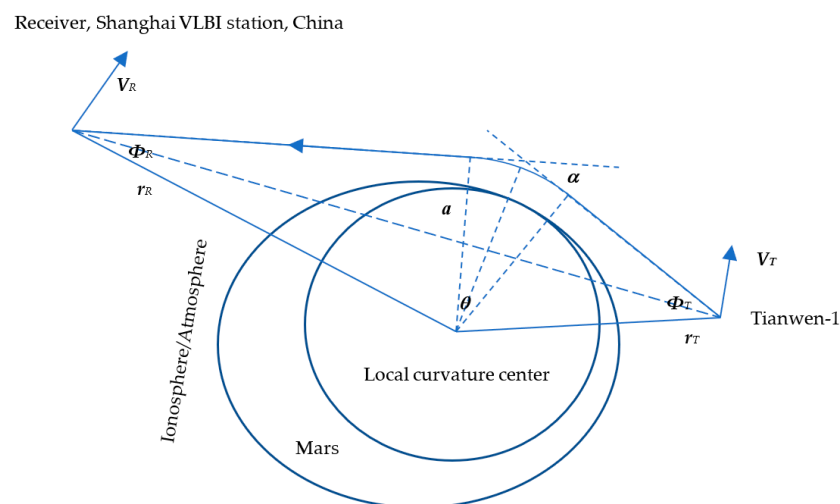

Figure 1. Geometric relationship of Tianwen-1 radio occultation.

The Shanghai station is used for the orbit determination of Tianwen-1 and is described in detail in the literature [12]. For receiving the downlink radio signals at 8431 MHz X-band for occultation, the VLBI receiver operates on two channels with a bandwidth of 2 MHz each and a sampling rate of 4 M Hz and 2-bit sampling resolution. The radio-science raw data can be directly transferred to a mass-storage device in Mark 5B format. Both the closed-loop mode and open-loop mode are used to track and retrieve the amplitude, carrier phase and carrier frequency of the occulted radio signal with the raw radio-science measurements, and to output their data stream with a compressed sampling rate of 100 Hz with bandwidth of 100 Hz.

In the Shanghai station, the meteorology observation system is enhanced with a newly installed water-vapor radiometer and GNSS receiver to promote the accuracy of the Earth's atmosphere and ionosphere delay correction in deep-space exploration [12,13].

2.2. Obseved Quantaties

The two data types (closed- and open-loop) can be generated simultaneously for the one-way radio link configuration. Both the closed-loop and open-loop data are given in UTC (Universal Time Coordinated) time with bandwidth of 100 Hz. The phase-observation equation is given in Equation (1) below:

$$\varphi = \rho + \rho_{rel} + c.\delta t_r - c.\delta t_{s/c} + \rho_{ion,E} + \rho_{atm,E} + \rho_{plasma,IP} + \rho_{ion} + \rho_{atm} + \cdots + \epsilon_t \quad (1)$$

where φ is the phase in m, ρ is the straight line distance between the Tianwen-1 and the receiver at the Shanghai ground station on Earth, ρ_{rel} is the relativistic delay due to the gravitation, c is light speed in vacuum, δt_r is the clock error of the receiver, $\delta t_{s/c}$ is the clock error of the Tianwen-1 spacecraft, $\rho_{ion,E}$ is the delay from Earth's ionosphere, $\rho_{atm,E}$ is the delay from Earth's atmosphere, $\rho_{plasma,IP}$ is the delay from the interplanetary plasma medium between Earth and Mars, ρ_{ion} is the delay from Mars's ionosphere, ρ_{atm} is the delay from Mars's atmosphere and ϵ_t is the thermal noise of the receiver.

2.3. Excess Phase

The excess phase is defined as the phase delay due to Mars's neutral atmosphere and ionosphere refraction in Equation (1). It can be derived by subtracting other items from the measured phase accurately as specified below.

$$\Delta\varphi = \rho_{ion} + \rho_{atm} \cong \varphi - (\rho + \rho_{rel} + \rho_{ion,E} + \rho_{atm,E} + \cdots + \epsilon_t) \quad (2)$$

In the right-hand side of Equation (2), the second item (the straight-line distance between Tianwen-1 and the receiver) and the third item (the relative theory delay) are calculated by the precise ephemeris of the planets (DE405) [14], Tianwen-1 and the precise position of the receiver at the Shanghai ground station. The relativistic delay is given and discussed in detail in the literature [15,16]. Since an ultra-stable hydrogen clock is used in the Shanghai ground station, and USO (ultra-stable oscillator) with a short-term frequency stability of 10^{-12} is onboard Tianwen-1, these two clock errors are neglected in the one-way RO mode here. The fourth and fifth items are removed with the simultaneously observed meteorology data and ionosphere data at the Shanghai ground station. The item of the interplanetary plasma in Equation (1) brings noise into the excess phase. Since temporal derivatives of the interplanetary plasma item are much less than the temporal derivatives of the Mars ionosphere and atmosphere items, and only the temporal derivatives are used in the following inversions processes, this item can be neglected in the following retrievals and hence is dropped in Equation (2).

After the excess-phase data are obtained, the excess doppler frequency due to the relative movement between Tianwen-1 and the receiver is obtained by their temporal differencing.

The major noise sources contributing to the excess phase and excess Doppler frequency errors are the thermal noises of the radio receiver on the ground and the transmitter on Tianwen-1 for one-way observations. The phase error assumed to be uncorrelated in time is related with its signal-to-noise ratio. The corresponding error in Doppler frequency is related with the phase error below:

$$\sigma_\varphi = \frac{1}{2\pi\sqrt{SNR}}, \sigma_{Doppler} = \frac{\sigma_\varphi}{\Delta t}, \quad (3)$$

where σ_φ is the standard deviation of a phase measurement (in cycles), SNR is the signal-to-noise ratio, $\sigma_{Doppler}$ is the standard deviation of a doppler frequency measurement (in Hz) and Δt is the time interval of measurements.

2.4. Bending Angle and Refracticity

Assuming Mars atmosphere and ionosphere are sphere-symmetric, the excess doppler is related with the RO geometric relationship shown in Figure 1.

$$\Delta f_d = \frac{f}{c}[(V_T \cdot e_T - V_R \cdot e_R) - (V_T - V_R) \cdot e_{TR}] \tag{4}$$

where Δf_d is the excess doppler frequency; f is the carrier frequency; e_T and e_R are the unit directional vectors of the incident radio ray at Tianwen-1 and the receiver, respectively; e_{TR} is the unit vectors of $(r_T - r_R)$; and r_T and r_R are the positions of Tianwen-1 and the receiver from the origin of the local curvature center, respectively.

The bending angle can be calculated by the following equation:

$$\alpha = \varnothing_R - \varnothing_T + \theta - \pi \tag{5}$$

For the sphere-symmetry atmosphere and ionosphere, the refractive index as a function of radius from the local curvature center, $n(r)$ is related with the bending angle through Abel transform [17]:

$$n(a) = \exp\left(\frac{1}{\pi} \int_a^\infty \frac{\alpha(x)dx}{\sqrt{x^2 - a^2}}\right) \tag{6}$$

where $a(=nr)$ is the impact parameter of the ray, r is ray periapse. The corresponding altitude can be calculated by $r - r_c$, where r_c is the radius of the local curvature in Figure 1.

In Mars's atmosphere and ionosphere medium, the radio-wave refractivity can be described as

$$N = (1 - n) \times 10^6 = C_1 n_a k + C_3 \frac{n_e}{f^2} \tag{7}$$

where n_a is the neutral number density, k is the Boltzmann constant, n_e is the electron density and C_1 and C_3 are constants.

2.5. Electron Density

The contributions of the radio-wave refractivity above 80 km are from Mars's ionosphere plasma, and below 60 km are from neutral atmosphere. The region between 60 km–80 km is the transit region. According to Equation (8), the electron density above 80 km can be obtained as

$$n_e = N \times \frac{f^2}{C_3} \tag{8}$$

2.6. Neutral Density, Temperature and Pressure

The neutral-atmosphere density below 60 km is obtained as follows:

$$n_a = \frac{N}{C_1 k} \tag{9}$$

Assuming that Mars's neutral atmosphere abides by the ideal gas law and the hydrostatic equilibrium, the pressure profile can be obtained by the integration specified below:

$$P(h) = P_u + \int_h^{z_u} n_a M g \, dh \tag{10}$$

where P_u ($=n_{au} k T_u$) is the top boundary pressure and can be calculated with the temperature (T_u) at the upper boundary with prior knowledge, z_u is the altitude of the top boundary, M ($=7.221 \times 10^{-26}$ kg) is the mean molecular mass density independent of altitude [18], g is the gravitational acceleration and h is the altitude.

The temperature profile is then calculated from density and pressure values by

$$T(h) = \frac{P}{n_a k} \qquad (11)$$

2.7. Vertical Resolution

The vertical resolution of the retrieved parameters is limited by the diameter of the first Fresnel zone of the propagating radio ray during the occultation. Since the distance of the tangent point of the radio ray is near Tianwen-1 and far from the Shanghai station, the first Fresnel zone is given by [19]:

$$d = 2\sqrt{\lambda D L_d} \qquad (12)$$

where λ is the wavelength of the radio wave, D is the distance form Tianwen-1 to the tangent point of the radio ray, L_d is the defocusing loss due to the ionosphere and atmosphere refraction. The defocusing loss is estimated by [20]:

$$L_d = \left(cos\alpha - D\frac{d\alpha}{da} \right)^{-1} \qquad (13)$$

2.8. Data

On 5 August 2021, Tianwen-1 RO's observation was made at around 7:08:21–7:14:15 UTC at Shanghai station as an experiment code of m1805x. The radio-science raw data and the open-loop/closed-loop tracking data were generated. The 100 Hz open-loop data is used for the following retrievals in the paper.

3. Results

The algorithm described in Section 2 is applied to the 100 Hz open-loop data to retrieve the excess phase, bending angle, refractivity, neutral-atmosphere parameters and ionosphere electron-density profiles.

3.1. Signal Amplitude and Excess Doppler

The tracked amplitude is given in Figure 2a. It is clear from Figure 2a that it is an egress RO event that the Tianwen-1 spacecraft comes out behind Mars. Before 140 s from the start time, Tianwen-1 is occulted by Mars and no signal is received, and the amplitude is close to 0.02 with random noise. After 150 s, the amplitude increases suddenly and reaches 0.07 with increased random noise. At 300 s, the signal-to-noise radio is about 22.43 dB, which corresponds to 0.0118 cycles of phase-measurement uncertainty and 1.18 Hz of frequency-measurement uncertainty according to Equation (3). When the raw data are smoothed with a 1 s window, their frequency-measurement uncertainty can be improved to 1.18 mHz, which is precise enough for the Mars ionosphere (~1 Hz) and neutral-atmosphere (~10 Hz) measurements.

The excess phase is derived from Equation (2) with the open-loop tracked carrier-phase data and Tianwen-1 precise orbit determination. The excess Doppler is easily obtained by differentiation of the excess phase and shown in Figure 2b. The excess Doppler is given versus the ray straight-line height between Tianwen-1 and Shanghai station above Mars's surface. Mars's neutral-atmosphere-induced excess Doppler increases to around several Hz versus the decreasing height below 70 km, as shown in Figure 2b. Above 80 km, the Mars-ionosphere-induced excess Doppler is not easily seen in Figure 2b.

The location of the tangent point of the straight-line ray closest to Mars's surface is estimated as (66.03°N, −161.49°E). At that occurrence time, its solar zenith angle is 87.7° with local time of 22.7 h. The season of the RO event occurrence is Mars's spring, with the seasonal longitude of $L_s = 81.3°$.
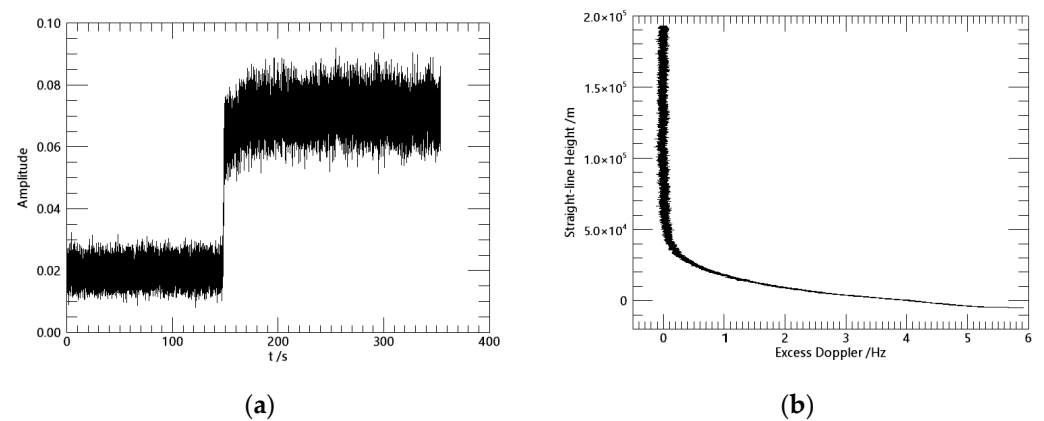
(a)

(b)

Figure 2. (**a**) Temporal series of open-loop tracked carrier amplitude since 07:08:21 on 5 August 2021; and (**b**) derived excess Doppler frequency versus the straight-line height between Tianwen-1 and Shanghai station above the Mars surface.

3.2. Bending Angle and Refractivity Profiles

The retrieved bending angle and refractivity profiles are given in Figure 3. The bending angle due to Mars's neutral atmosphere is clearly seen and reaches about 220 micro-radian, shown in Figure 3a. The refractivity is obtained by Equations (6) and (7) and shown in Figure 3b. Mars's ionosphere medium is a dispersive medium and contributes to Mars's refractivity above 80 km. The neutral-atmosphere medium is a nondispersive medium and contributes to Mars's refractivity below 60 km [11]. In Figure 3b, Mars's neutral atmospheric refractivity reaches 4.7 at the bottom. A zoomed refractivity within Mars's ionospheric height ranges is depicted in Figure 3c. It is clear to see that the X-band radio wave's refractivity due to Mars's ionosphere refraction is very small but evident.
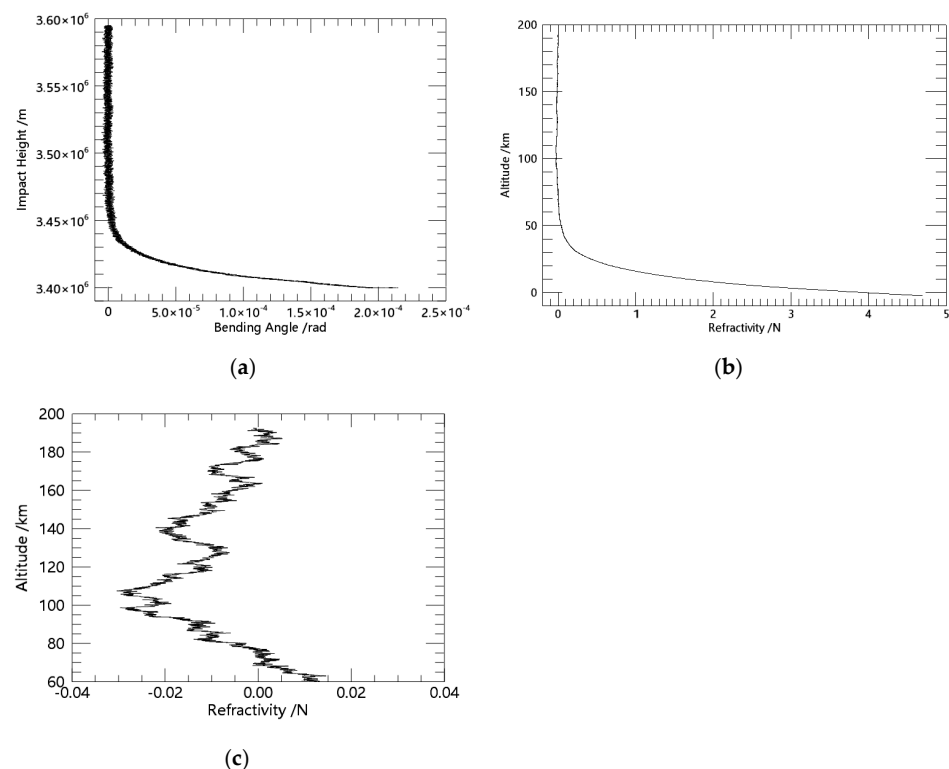

(a)

(b)

(c)

Figure 3. (**a**) Retrieved bending angle versus the ray impact height, (**b**) retrieved refractivity versus altitude, and (**c**) zoomed Mars ionosphere refractivity.

The vertical resolutions of the bending angle and refractivity profiles, and the following ionospheric/atmospheric parameters profiles are estimated in the range of 1.33–1.34 km, according to Equations (12) and (13).

3.3. Mars Ionospheric Electron-Density Profile

Mars's ionosphere electron density above 80 km is then obtained with the refractivity profile data shown in Figure 3c and specified by Equation (8), as shown in Figure 4. It can be found that M1(M2) layer has a peak height of ~140 km (~105 km) with peak density of ~3.7×10^{10} el/m^3 (5.3×10^{10} el/m^3).
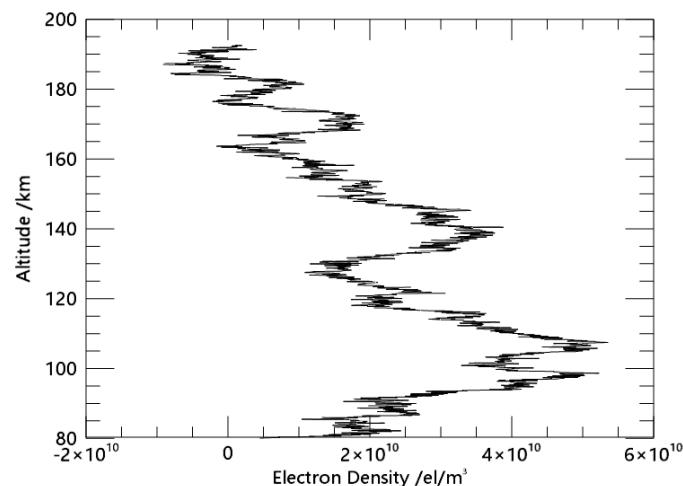

Figure 4. Retrieved Mars ionosphere electron-density profile.

Mars's ionosphere below 200 km is in photochemical equilibrium and depends on the solar zenith angle [21–24]. The solar zenith angle of the RO event is about 87.7° as mentioned above, which means that the light penetrates a long distance in the atmosphere and its ionizing ability becomes weak. The weak ionization is the reason why the observed ionospheres of M1 and M2 are very weak, as shown in Figure 4. The M1 peak corresponds to solar EUV irradiance ionizations and the M2 peak is related to the solar soft X-ray ionizations.

The electron-density profile in Figure 4 shows oscillation phenomena. Siddlea et al. (2019) [25] have specified the gravity waves in Mars's upper atmosphere above 120 km using in situ data from NGIMS onboard MAVEN. They have obtained that the atmospheric gravity waves have amplitudes of around 10% with vertical wavelengths of around 10–30 km. The atmospheric gravity waves are believed to couple with the plasma in the regions through dynamical and photochemical processes, and to induce oscillations in electron-density profiles as observed in Figure 4.

It is usual that the M1 peak density is greater than M2. However, it is interesting to find out in Figure 4 that M1 peak density is less than M2. Besides their different ionization sources, the dynamical coupling processes between the gravity waves and electron densities in Mars's upper atmosphere might be the reasons.

3.4. Mars Atmospheric Profiles

The refractivity profile below 60 km shown in Figure 3b is used to retrieve the atmospheric density, pressure and temperature profiles with Equations (9)–(11). The results are given in Figure 5. The top boundary is taken at z_u = 60 km, and the top temperature is taken to be Tu = 140 K based on prior knowledge. The error in the artificial top boundary temperature will be greatly reduced when downward integration is 10 km away, as given with Equation (10) [1,26]. The density and pressure profiles show exponential decreases versus increasing altitude shown in Figure 5a,b. The bottom pressure is about 800 Pa, which agrees well with previous RO measurements [9].
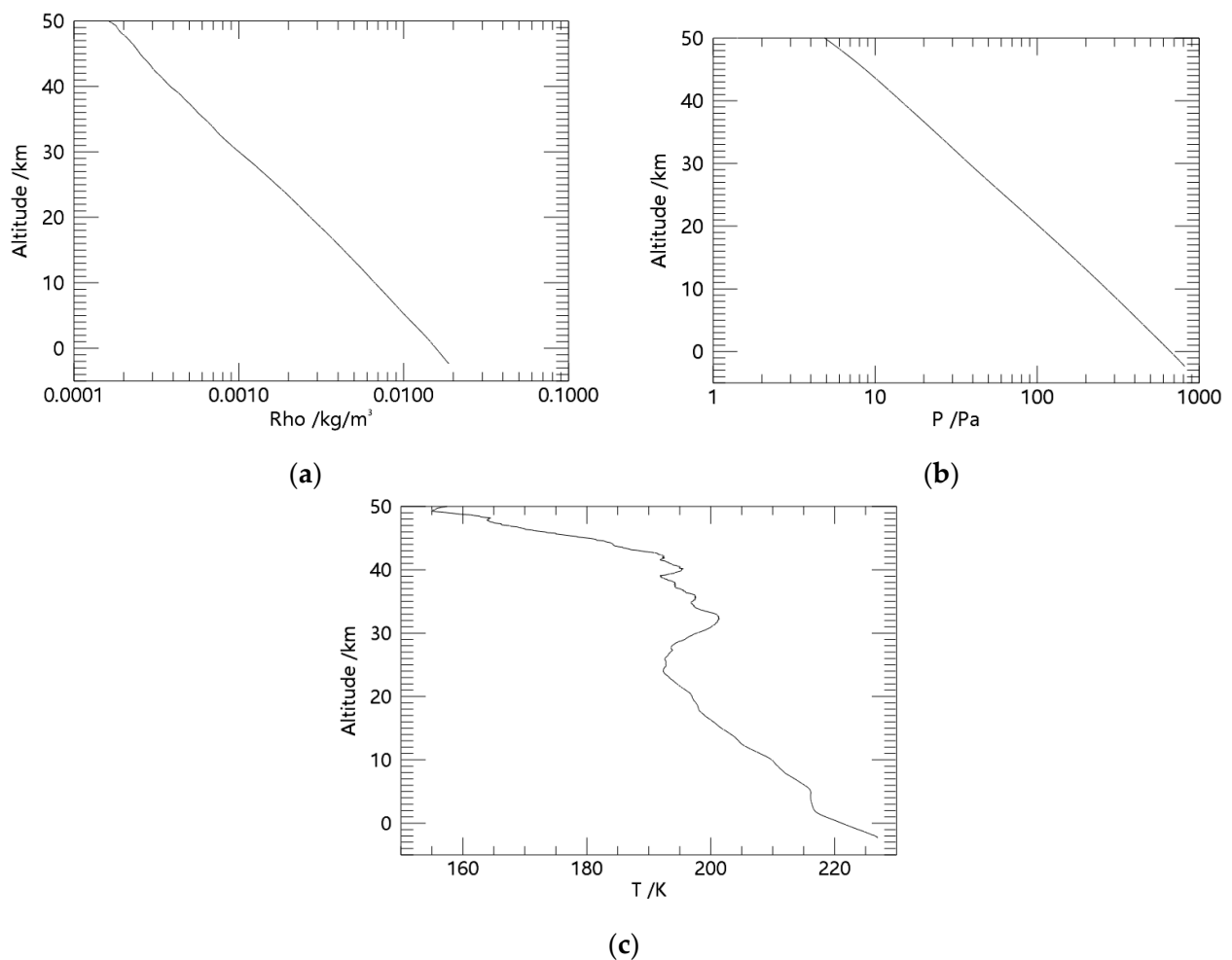
Figure 5. (**a**) Retrieved atmospheric density, (**b**) pressure and (**c**) temperature profiles.

The temperature profile in Figure 5c shows typical Mars spring atmospheric features at 66.03°N clearly. The temperature is about 226.9 K at the bottom altitude of about −2.35 km. It decreases with increasing altitude to 192 K at about 24 km. Above 24 km, it grows with altitude and reaches a peak of 202 K at about 33 km. Above 40 km, the temperature decreases with increasing altitude again and has a value of 155 K near 50 km altitude.

At the bottom part of the profile below 5 km, the planetary boundary layer (PBL) feature is clearly seen. Within the PBL, the temperature decreases with height rapidly with a vertical lapse rate greater than 2 K/km till to altitude of 1.35 km, and it remains almost constant versus height up to the PBL top of about 5 km. Dayside PBL is produced by the response of the atmosphere to the solar heating of the surface. The PBL varies strongly with time of day, location and season. Vertical transport of heat and momentum by the PBL has a large impact on the temperature structure and circulation of the atmosphere [27].

The temperature inversion layer within 24 km–40 km is related with the ozone layer in Mars's atmosphere, which absorbs solar UV irradiances and heats/warms the atmosphere. The detection of ozone is achieved by UV spectrometry [28,29]. Ozone shows strong seasonal, latitudinal and local variations [30].

The wave-like structures can be clearly found in the temperature profile in Figure 5c, which implies that the atmospheric wave activities are rich in Mars atmosphere, as their induced oscillations seen in Figure 4.

4. Conclusions

The first RO event observation at X-band downlink between Tianwen-1 and Shanghai station was completed successfully at 7:08:21–7:14:15UTC on 5 August 2021. The Tianwen-1 one-way single-frequency RO technique was developed to retrieve excess Doppler frequency, bending angle, refractivity, electron density, neutral mass density, pressure and temperature profiles. The Mars ionospheric electron-density profile clearly shows M1 and M2 layers. The Mars atmospheric density and pressure profiles show reasonable features of exponential decreases with height. The temperature profile gives clearly the structure of PBL, Mars's troposphere and 'stratosphere', and the phenomena of atmospheric waves. The conception and capability of Mars RO observation with the Chinese Tianwen-1 is proved by the results.

More RO observation experiments and their coordination with other active Mars spacecraft (MEX et al.) are expected to yield further Mars science discoveries.

Author Contributions: X.H. conceptualized the work, programmed the Tianwen-1 one-way single-frequency RO algorithm and wrote the manuscript; X.W. verified the RO retrieval algorithm; S.S. and W.Z. made the Earth ionosphere and atmosphere observations and corrections on Shanghai station; M.M. organized the observation of m180x, found the occultation phenomenon and provided the data; Q.X. and Q.Z. programmed the 100 Hz open-loop/closed-loop tracking code and prepared the data; L.L. verified the RO retrieval algorithm and provided financial support; C.X. verified the retrieved Mars ionosphere and atmosphere profile data; X.L. was responsible for the observation between Tianwen-1 and Shanghai station; C.W. oversaw the Tianwen-1 RO scientific goals and aims; Q.L. was responsible for the observation in Shanghai station and discussed the RO event observation chances; L.C., G.C., J.C. and M.W. coordinated the observation between Tianwen-1 and Shanghai station and provided the precise ephemeris of Tianwen-1; P.L. provided the prior ephemeris and technical supports for the observation of m1805x; Z.C. performed calculations of the observation schedule of m1805x; B.X. carried out the observation at Shanghai station with the 25 m antenna; J.Y. interpreted the retrieved Mars atmosphere profiles and provided part of the financial support; C.T. worked on the excess-phase data-extraction algorithm; D.L., S.Z. and Z.L. participated in the data retrieval and interpretation. All authors made contributions to all technical and scientific discussions. All authors have read and agreed to the published version of the manuscript.

Data Availability Statement: The data presented in this study are available on request from the corresponding author.

Conflicts of Interest: The authors declare that they have no conflict of interest.

References

1. Withers, P. Prediction of uncertainties in atmospheric properties measured by radio occultation experiments. *Adv. Space Res.* **2010**, *46*, 58–73. [CrossRef]
2. Hinson, D.P.; Asmar, S.W.; Kahan, D.S.; Akopian, V.; Haberle, R.M.; Spiga, A.; Schofield, J.T.; Kleinböhl, A.; Abdou, W.A.; Lewis, S.R.; et al. Initial results from radio occultation measurements with the Mars Reconnaissance Orbiter: A nocturnal mixed layer in the tropics and comparisons with polar profiles from the Mars Climate Sounder. *Icarus* **2014**, *243*, 91–103. [CrossRef]
3. Ao, C.O.; Edwards, C.D.; Kahan, D.S.; Asmar, S.W.; Mannucci, A.J. A first demonstration of Mars crosslink occultation measurements. *Radio Sci.* **2015**, *50*, 997–1007. [CrossRef]
4. Withers, P.; Felici, M.; Mendillo, M.; Moore, L.; Narvaez, C.; Vogt, M.F.; Oudrhiri, K.; Kahan, D.; Jakosky, B.M. The MAVEN Radio Occultation Science Experiment (ROSE). *Space Sci. Rev.* **2020**, *261*, 61. [CrossRef]
5. Kliore, A.; Cain, D.L.; Levy, G.S.; Eshleman, V.R.; Fjeldbo, G.; Drake, F.D. Occultation experiment: Results of the first direct measurement of Mars's atmosphere and ionosphere. *Science* **1965**, *149*, 1243–1248. [CrossRef]

6. Zhang, R.Q.; Geng, H.; Sun, Z.Z.; Li, D.; Zhong, W.A.; Li, H.T.; Cui, X.F.; Liu, J.J. Technical innovations of the Tianwen-1 Mission. *Acta Aeronaut. Astronaut. Sin.* **2022**, *43*, 626689. (In Chinese) [CrossRef]

7. Chen, L.; Zhao, C. China successfully launched its first Mars mission, Tianwen 1. *Aerosp. China* **2020**, *21*, 2.

8. Pätzold, M.; Häusler, B.; Tyler, G.L.; Andert, T.; Asmar, S.W.; Bird, M.K.; Dehant, V.; Hinson, D.P.; Rosenblatt, P.; Simpson, R.A.; et al. Mars Express 10 years at Mars: Observations by the Mars Express Radio Science Experiment (MaRS). *Planet. Space Sci.* **2016**, *127*, 44–90. [CrossRef]

9. Hu, X.; Wu, X.C.; Gong, X.Y.; Wang, X.; Xu, Q.C. Simulation of the Mars ionosphere radio occultation experiments. *Acta Astromica Sin.* **2009**, *50*, 301–311.

10. Zhang, S.J.; Cui, J.; Guo, P.; Li, J.L.; Ping, J.S.; Jian, N.C.; Zhang, K.F. Martian electron density profiles retrieved from Mars Express dual-frequency radio occultation measurements. *Adv. Space Res.* **2015**, *55*, 2177–2189. [CrossRef]

11. Withers, P.; Moore, L.; Cahoy, K.; Beerer, I. How to process radio occultation data: 1. From time series of frequency residuals to vertical profiles of atmospheric and ionospheric properties. *Planet. Space Sci.* **2014**, *101*, 77–88. [CrossRef]

12. Liu, Q.H.; Huang, Y.; Shu, F.C.; Wang, G.; Zhang, J.; Chen, Z.; Li, P.; Ma, M.; Hong, X. VLBI technique for the orbit determination of Tianwen-1. *Sci. Sin-Phys. Mech. Astron.* **2022**, *52*, 239507. (In Chinese) [CrossRef]

13. Zhou, W.L.; Song, S.L.; Li, P.J.; Zhang, Z.; Huang, C.; Huang, Y.; Wang, G. Ionsopheric TEC correction for VLBI based on GNSS density network. *J. Deep Space Explor.* **2020**, *7*, 362–370. (In Chinese)

14. Standish, E.M. "JPL Planetary and Lunar Ephemerides," DE405/LE405. Interoffice memorandum: JPL IOM 312. F–98-048, 26 August 1998. Available online: ftp://ssd.jpl.nasa.gov/pub/eph/planets/ioms/de405.iom.pdf (accessed on 17 February 2022).

15. Zhu, J. The influence of gravitational deflection and retardation on VLBI time delay. *Acta Astron. Sin.* **1990**, *31*, 349–355.

16. Yang, Z.G.; Zhao, M. Discussion and comparison of various VLBI relativistic time delay models. *Acta Astron. Sin.* **1992**, *33*, 201–211.

17. Fjeldbo, G.; Eshleman, V.R. The Atmosphere of Mars Analyzed by Integral Inversion of the Mariner IV Occultation Data. *Planet. Space Sci.* **1968**, *16*, 1035–1059. [CrossRef]

18. Hinson, D.P.; Simpson, R.A.; Twicken, J.D.; Tyler, G.L.; Flasar, F.M. Initial results from radio occultation measurements with Mars Global Surveyor. *J. Geophys. Res.* **1999**, *104*, 26997–27012. [CrossRef]

19. Imamura, T.; Ando, H.; Tellmann, S.; Pätzold, M.; Häusler, B.; Yamazaki, A.; Sato, T.M.; Noguchi, K.; Futaana, Y.; Oschlisniok, J.; et al. Initial performance of the radio occultation experiment in the Venus orbiter mission Akatsuki. *Earth Planet Space* **2017**, *69*, 137. [CrossRef]

20. Eshleman, V.R. The radio occultation method for the study of planetary atmospheres. *Planet Space Sci.* **1973**, *21*, 1521–1531. [CrossRef]

21. Singh, R.N.; Prasad, R. Production of Dayside Ionosphere of Mars. *J. Astrophys. Astron.* **1983**, *4*, 261–269. [CrossRef]

22. Martinis, C.R.; Wilson, J.K.; Mendillo, M.J. Modeling day-to-day ionospheric variability on Mars. *J. Geophys. Res.* **2003**, *108*, 1383. [CrossRef]

23. Nagy, A.F.; Grebowsky, J.M. Current understanding of the aeronomy of Mars. *Geosci. Lett.* **2015**, *2*, 5. [CrossRef]

24. Withers, P.; Felici, M.; Hensley, K.; Mendillo, M.; Barbinis, E.; Kahan, D.; Oudrhiri, K.; Girazian, Z. The ionosphere of Mars from solar minimum to solar maximum: Dayside electron densities from MAVEN and Mars Global Surveyor radio occultations. *Icarus* 2021, *in press*. [CrossRef]

25. Siddlea, A.G.; Mueller-Wodarga, I.C.F.; Stoneb, S.W.; Yelle, R.V. Global characteristics of gravity waves in the upper atmosphere of Mars as measured by MAVEN/NGIMS. *Icarus* **2019**, *333*, 12–21. [CrossRef]

26. Hajj, G.A.; Kursinski, E.R.; Romans, L.J.; Bertiger, W.I.; Leroy, S.S. A technical description of atmospheric sounding by GPS occultation. *J. Atmos. Sol.-Terr. Phys.* **2002**, *64*, 451–469. [CrossRef]

27. Hinson, D.P.; Tyler, D.; Lewisd, S.R.; Pätzold, M.; Tellmann, S.; Häusler, B.; Tyler, G.L. The martian daytime convective boundary layer: Results from radio occultation measurements and a mesoscale model. *Icarus* **2019**, *326*, 105–122. [CrossRef]

28. Barth, C.A.; Hord, C.W.; Stewart, A.I.; Lane, A.L.; Dick, M.L.; Anderson, G.P. Mariner 9 Ultraviolet Spectrometer Experiment: Seasonal Variation of Ozone on Mars. *Science* **1973**, *179*, 795–796. [CrossRef] [PubMed]

29. Krasnopolsky, V.A.; Parshev, V.A.; Krysko, A.A.; Rogachev, V.N. *Structure of the Mars Lower and Middle Atmosphere Based on Mars 5 Ultraviolet Photometry Data*; Academy of Sciences (USSR): Moscow, Russia, 1979.

30. Encrenaz, T. The Atmosphere of Mars as constrained by remote sensing. *Space Sci. Rev.* **2001**, *96*, 411–424. [CrossRef]